Published in final edited form as:
Dev Dyn. 2011 June ; 240(6): 1548–1557. doi:10.1002/dvdy.22622.

Heart chamber size in zebrafish is regulated redundantly by duplicated *tbx2* genes

Anya Sedletcaia and **Todd Evans***
Department of Surgery Weill Cornell Medical College New York, NY 10065

Abstract

The Tbx2 transcription factor is implicated in growth control based on its association with human cancers. In the heart, Tbx2 represses cardiac differentiation to mediate development of the atrioventricular canal (AVC). The zebrafish genome retains two *tbx2* genes, and both are required for formation of the AVC. Here we show that both genes are also expressed earlier in the primitive heart tube, and we describe a previously unrecognized role for Tbx2 in promoting proliferation of presumptive myocardium at the heart tube stage. In contrast to single knockdowns, depletion of both gene products causes chamber defects, resulting in an expanded atrium and a smaller ventricle, associated with decreased proliferation of ventricular cardiomyocytes. The phenotype correlates with changes in the expression for known cardiac growth factors. Therefore, in zebrafish, two *tbx2* genes are functionally redundant for regulating chamber development, while each gene is required independently for development of the AVC.

Keywords

cardiogenesis; T-box; cardiomyocytes; *nppa*; *ndrg4*

INTRODUCTION

In zebrafish, specified cardiac progenitors are located in bilateral stripes within anterior lateral plate mesoderm. These cell populations migrate medially and fuse at the midline forming a cardiac cone at 19.5 hours post fertilization (hpf), through a process called “cardiac fusion” (Zaffran and Frasch, 2002). Cells from the cone “telescope” to form an extended tubular structure called the primitive heart tube, with regions specified as presumptive atrial or ventricular tissue. In the first obvious break of symmetry, the heart tube “jogs” to the left and begins beating by 24 hpf. Around 36 hpf the heart tube undergoes a more extensive morphogenetic process called cardiac looping (Bakkers et al., 2009), which is essential for orienting the eventual positions of the atrium and ventricle in the mature heart. At the junction of atrial and ventricular myocardium, endocardial cushion tissue grows out at the atrioventricular canal (AVC) and from this non-myocardial tissue valves develop between the two chambers (Boogerd et al., 2009; Yelon, 2001). Regulated signals including those related to Wnt, BMP, Notch, and RA pathways tightly control each of these steps of cardiac development (Joziasse et al., 2008; Zaffran and Frasch, 2002). Mediating response to these signals is a complex network of cardiac transcription factors, including those comprising GATA, HAND, NKX2 and T-box families (Schoenebeck and Yelon, 2007). This network in turn regulates proliferative cues that modulate chamber outgrowth and formation of the AVC, while proliferation is inhibited at the outflow tract (OFT) and the inflow tract (IFT).

*Corresponding author: 1300 York Ave. LC-709 212 746-9485 212 746-7378 (fax) tre2003@med.cornell.edu.

Members of the T-box family of transcription factors share an approximately 200 amino acid DNA-binding domain called the T-domain. *Brachyury* (T) was the first family member identified at the locus of a murine loss-of-function mutation that causes a short tail phenotype (Abrahams et al., 2010; Chapman et al., 1996). Over 17 family members have since been identified and they are expressed in a variety of tissues from embryogenesis to adulthood (Hoogaars et al., 2007). Mutations or deletions of some family members are linked to human genetic disorders. Thus, DiGeorge syndrome is caused by a deletion at 22q11, characterized by thymic hypoplasia, cleft palate, and cardiovascular anomalies. Haploinsufficiency of Tbx1 in mice largely recapitulates cardiac defects seen in patients (Hoogaars et al., 2007; Merscher et al., 2001; Yamagishi et al., 2003). Mutation of TBX3 causes ulnar-mammary syndrome, an autosomal-dominant disorder characterized by hypoplasia of upper limbs, as well as mammary and apocrine glands (Abrahams et al., 2010; Klopocki et al., 2006). Haploinsufficiency of Tbx5 causes Holt-Oram syndrome, an autosomal dominant disorder with skeletal and cardiac abnormalities (Boogerd et al., 2009; Li et al., 1997; Liu et al., 2009). Tbx5 deficient mice exhibit conduction and septation defects, as well as hypoplasia of the left ventricle and atrium (Bruneau et al., 2001; Harrelson et al., 2004).

Tbx2 encodes a T-box factor that has been associated with growth control. TBX2 is over-expressed in melanoma cells (Vance et al., 2005), and is amplified and over-expressed in BRCA1 and BRCA2 mutant breast cancer cells (Mahlamaki et al., 2002; Sinclair et al., 2002) and pancreatic cancer cell lines (Mahlamaki et al., 2002). TBX2 has both repressor and activator domains (Abrahams et al., 2010; Paxton et al., 2002) and blocks chamber differentiation by repressing chamber-specific genes (Christoffels et al., 2004). In mice, *Tbx2* is expressed in non-chamber myocardium, namely the OFT, AVC, and IFT (Boogerd et al., 2009; Christoffels et al., 2004; Habets et al., 2002). In these areas it blocks chamber differentiation programs, represses proliferation, and thereby generates constrictions between chambers, modulating heart morphogenesis (Abrahams et al., 2010). *Tbx2* null embryos die due to cardiovascular defects caused by the absence of AVC, dilated ventricle, and failure of OFT septation, while heterozygotes are viable and fertile (Harrelson et al., 2004).

In zebrafish two *tbx2* genes are retained in the genome following gene duplication, designated *tbx2a* and *tbx2b*, sharing 79.5% identity. The *tbx2a* transcripts are detected in the linear heart tube but are subsequently restricted to the AVC and OFT by 42 hpf (Ribeiro et al., 2007). Morpholino mediated knockdown showed looping defects due to the loss of AVC constriction. The *tbx2b* transcripts were reported at 48 hpf in the embryonic AVC and OFT. The *tbx2b* morphants also lack the AVC at 40 hpf (Chi et al., 2008). Thus, the requirement for both *tbx2* genes in zebrafish AVC development has been well described. However, since *tbx2* has been duplicated and retained in zebrafish as two separate genes, it is possible that functions for either gene, in addition to roles in AVC development, might be compensated in loss-of-function experiments by the sister gene. Here we show that both *tbx2* genes are expressed in the linear heart tube, and we provide evidence that, in addition to regulating proper AVC formation, Tbx2 is also important, at an earlier stage, for regulating myocardial chamber development.

RESULTS

Transcripts for both *tbx2a* and *tbx2b* are expressed in presumptive chamber myocardium

It was reported previously that *tbx2a* transcripts are expressed throughout the linear heart tube of zebrafish embryos at 31 hpf (Ribeiro et al., 2007). Yet loss-of-function studies for *tbx2a* showed functions only in the non-myocardial AVC. Alignment of Tbx2a and Tbx2b proteins revealed that they share 79.5% sequence identity (data not shown). We considered

that loss-of-function for *tbx2a* in chambers could be compensated by this closely related sister gene, assuming they are co-expressed. Therefore, we examined and compared the expression patterns of *tbx2a* and *tbx2b* during early stages of cardiac development, by *in situ* hybridization experiments. This revealed that both *tbx2a* and *tbx2b* transcripts are expressed throughout the linear heart tube, as detected by *in situ* hybridization, by 36 hpf (Fig. 1A,C). Both transcript patterns are subsequently restricted to the AVC region by 3 days post fertilization (dpf; Fig. 1B,D). Since expression in the AVC is challenging to visualize at this stage, we confirmed that the restriction is apparent already at 2 dpf, by comparison to the *bmp4* transcript pattern that marks the AVC (Fig. 1G-I). Since previous studies of Tbx2 focused only on its function during AVC development, yet both sister genes are expressed earlier in the heart tube, we further investigated a possible role for chamber development.

Blocking expression of both *tbx2* genes generates cardiac defects that are different from *tbx2a* or *tbx2b* single knockdowns

To best assure efficient and equivalent depletion of both Tbx2 proteins, we took advantage of the high sequence identity for the two genes to design a single antisense morpholino oligomer (MO2ab) predicted to bind to a common sequence near the ATG translation initiation codon for each transcript (Supplemental Fig. S1). To test the efficacy of targeting, chimeric cDNAs were constructed representing each gene, comprised of the 5′ UTR and initial coding region, including the morpholino binding site, fused in frame with GFP. Injection into fertilized eggs of RNA derived from these constructs, encoding Tbx2ab-GFP or Tbx2b-GFP, generates embryos that express high levels of GFP in all tissues. In both cases, co-injection of 2 ng of MO2ab is sufficient to eliminate detectable GFP expression, indicating that MO2ab efficiently binds to both transcripts to effectively block translation (Fig. 2).

The phenotypes of single *tbx2a* and *tbx2b* morphants are well documented in the literature (Chi et al., 2008; Ribeiro et al., 2007). We compared the embryonic phenotype caused by injection of MO2ab with morpholinos that target only *tbx2a* (MO2a) or *tbx2b* (MO2b). The *tbx2ab* morphants have hypoplastic eyes and brain, and a shorter AP axis. These phenotypes were previously described in *tbx2* morpholino-mediated knockdowns (Fong et al., 2005; Gross and Dowling, 2005) and further verify the effectiveness of the MO2ab morpholino. Like the single morphants, the *tbx2ab* double morphants also fail to develop a normal AVC, as expected (with an expanded domain of *bmp4* expression and morphological disruption noted in the *tie2:gfp* reporter fish, data not shown). However, with respect to heart development, the *tbx2ab* morphants develop pericardial edema as early as 24 hpf (Fig. 3A), which becomes more prominent by 2 dpf and 3 dpf (Fig. 3B,C). We compared morphants at 24 hpf for jogging defects. By this time, 95% of wild type embryonic hearts jog to the left. The single *tbx2a* or *tbx2b* morphants display heart jogging appropriately to the left side, 94% and 88% of the time, respectively, while this is the case for only 23% of *tbx2ab* double morphant embryos. Rather, 60% of *tbx2ab* morphant hearts fail to jog and remain at the midline, and the remaining 17% jog to the right (Fig. 4A). We found no evidence for direct defects in left-right patterning (for example, *lefty2* expression is normal, data not shown), suggesting that the jogging defect is caused indirectly by abnormal heart tube morphology. We note that these morphological defects occur earlier than the time we first reliably detect *tbx2* transcripts by *in situ* hybridization. We believe this reflects limitations in the assay. The *tbx2* transcripts are readily detected by qPCR in whole embryos by 24 hpf (Supplemental Fig. S2). In addition, we purified using flow cytometry 24 hpf cardiomyocytes from *myl7:gfp* reporter fish embryos. Using degenerate oligomers we cloned out PCR products predicted to encode the Tbox domain, and found representation of *tbx2a* and *tbx2b* in this pool. Finally, we used deep sequencing of 24 hpf purified cardiomyocyte mRNA and verified *tbx2a* and *tbx2b* transcripts were readily quantified (BPKM 4.7 and 4.6,

respectively). Therefore, the *tbx2* genes are expressed in the heart tube cardiomyocytes earlier than we can document by *in situ* hybridization. Signals below the threshold of *in situ* hybridization noise may still be functionally relevant. Therefore, depletion of both *tbx2* gene products generates morphological defects that are not seen in either single morphant, indicating that they are functionally redundant.

The *tbx2ab* double morphants have enlarged atria and small ventricles

In order to characterize the apparent morphogenetic defect caused by targeting both *tbx2* genes, we repeated the analysis using transgenic *myl7:gfp* (previously called *cmlc2:gfp*) reporter fish that express GFP in cardiomyocytes. Compared to control injected or uninjected embryos, at 24 hpf the morphants have normally formed (albeit non-jogging) heart tubes (Fig. 4B,E). By 2 or 3 dpf cardiac chamber defects are obvious; specifically the *tbx2ab* morphant hearts have an enlarged balloon-like atrium with a smaller ventricle (Fig. 4C,D,F,G). While 132/135 (98%) of wildtype embryos were scored as normal, 110/172 (64%) of *tbx2ab* morphant embryos have an enlarged atrium and a small ventricle at 3 dpf. This cardiac phenotype is distinct from those described for either *tbx2a* or *tbx2b* single morphants, and this was confirmed by our own experiments (Fig. 4H-K). The single morphants exhibit heart tube looping defects due to the lack of AVC formation, but chamber sizes are not grossly affected. We quantified chamber defects comparing *tbx2ab* double morphants and wildtype embryos by measuring the size of cardiac chambers using embryos derived from the *myl7:gfp* reporter fish. At 1 dpf there is no difference in size between morphant and wildtype hearts (Fig. 5A, B, E). By 2 dpf morphant atria are twice the size of wildtype stage-matched embryos (Fig. 5A,C,F) and this chamber size difference is maintained at 3 dpf (Fig. 5A,D,G). Ventricular chamber size is not affected in morphant embryos at 2 dpf; however, by 3 dpf morphant ventricles are just over 20% smaller (Fig. 5A,D,G). Therefore, the two *tbx2* genes are functionally redundant for regulating chamber size.

The *tbx2ab* morphants are altered in proliferation of cardiomyocytes

We next used embryos derived from transgenic *dsRed:nuc-myl7* reporter fish line to quantify cardiomyocytes in wildtype and morphant hearts, in order to determine if differences in the size of chambers is due to changes in cell number. In embryos from this transgenic line, nuclear RFP expression is readily visible in cardiomyocytes around 2 dpf. At this time, there are approximately 40% fewer cardiomyocytes (average of 104 cells) in the *tbx2ab* morphant heart tubes compared with wildtype embryos (average of 176 cells; Fig. 6A,B,D). The numbers at 3 dpf are similar, with no significant difference between the numbers of atrial cardiomyocytes in morphant (average of 65 cells) and wildtype embryos (average of 64 cells), while there are 35% fewer ventricular cardiomyocytes in the morphants compared to wildtype embryos (average of 72 and 110 cells, respectively; Fig. 6A,C,E). Because a constriction that delineates the presumptive chambers can be seen at 2 dpf, we repeated the study using an independent set of embryos to evaluate presumptive chamber-specific differences at this early time point. This analysis suggests that the difference in cell numbers can likely be accounted for by a significant deficit in morphant embryos of cardiomyocytes of the presumptive ventricle (average of 84 compared to 114 in wildtype), while cell numbers in the presumptive atrium are not significantly changed (Fig. 7).

The relative decrease in cardiomyocyte number in the morphants does not appear to be due to cell death, since staining by TUNEL or acridine orange showed no increase in labeled cells in the heart (data not shown). We therefore tested if the phenotype could be attributed to defects in cardiomyocyte proliferation. For this purpose, embryos were pulse labeled with BrdU, followed by dual-immunohistochemistry to identify BrdU+ cardiomyocytes, based on

co-reactivity to the MF20 antigen. At 32 hpf, the number of double-labeled cells in the *tbx2ab* morphant embryos is reduced (Fig. 8). This result was confirmed in several independent experiments. Although the exact number of double-positive cells varies depending on BrdU labeling efficiency, there was a consistent statistically significant relative decrease in the double morphants compared to controls. We repeated this assay and co-stained BrdU pulse-labeled embryos with the S46 antibody, which marks specifically the atrial cells. In this case we did not find a statistically significant difference in the double-labeled cells, comparing wildtype and double morphant embryos (Fig. 9). This observation is consistent with our finding that the number of cells in the atrium is not different in the 2 dpf or 3 dpf morphants compared to controls. Therefore, the relative decrease in the number of cardiomyocytes found by 2-3 dpf in the heart tube of *tbx2ab* morphant embryos appears to be caused by a cell proliferation defect in the presumptive ventricle. By 48 hpf the change in cardiomyocyte number can be fully accounted for by the ventricle, and the data indicates that the two *tbx2* genes redundantly regulate cardiomyocyte proliferation at the heart tube stage.

Changes in gene expression of growth factors are consistent with a role for Tbx2 in chamber development

To investigate the molecular mechanism underlying chamber defects seen in the *tbx2ab* morphant embryos, we used *in situ* hybridization to examine the expression pattern of cardiac markers. In the *tbx2ab* morphants, specification of cardiac tissue occurs normally, since the expression patterns for early precardiac markers *nkx2.5*, *gata4*, *gata5*, and *gata6* are normal (data not shown). At 24 hpf, the chamber markers *myl7* (heart tube), *amhc* (presumptive atrial), and *vmhc* (presumptive ventricular) are expressed in morphant embryos similar to wildtype, except that the patterns now reflect morphological changes. Therefore, the rostral region of the heart tube that will form the ventricle (indicated by *myl7* and *vmhc*) is smaller, while the caudal pre-atrial pattern indicated by *myl7* and *amhc* is broadened (Supplemental Fig. S3). In contrast, based on these markers the morphology of *tbx2a* or *tbx2b* single morphants is undisturbed (Fig. S3). Although specification appears to be normal, we evaluated whether normal proportions of chamber-specific progenitors are present at pre-heart tube stages. Expression domains at the 19.5 hpf cardiac cone stage for chamber-specific markers *amhc* and *vmhc* are not changed in morphants compared to controls (Supplemental Fig. S4). The morphology of the *amhc* pattern is slightly disturbed, but the staining area is normal, and notably the *vmhc* patterns are indistinguishable. The data is consistent with an interpretation of the heart tube phenotype caused by disturbed morphology and not defects in chamber progenitor cell numbers.

The *nppa* gene (*natriuretic peptide precursor a*, formerly known as *anf, atrial natriuretic factor)* is expressed in the outer curvature (OC) of myocardium. Transcript levels for *nppa* are enhanced in the OC of *haf* mutants (lacking Vmhc protein and ventricular contractility), and this leads to increased cell surface area (Auman et al., 2007). Since the *tbx2ab* morphants have enlarged atria, but with normal cell numbers, we tested if *nppa* gene expression is altered. *In situ* hybridization experiments suggest that as early as 24 hpf the *tbx2a* morphants have increased expression of *nppa* in the atrial region, compared to wildtype embryos (Supplemental Fig. S5). However, the pattern in the double morphant already suggests a morphological change in the presumptive atrium. It is possible that this reflects a developmental delay in heart tube formation, although the morphology does not recover; in other words, at later times the double morphants do not display a normal 24 hpf heart tube. At any rate, this apparent increase in *nppa* expression levels in the *tbx2a* morphant is not maintained by 48 hpf (data not shown, but see qPCR data below), while in the double morphants by 48 hpf the expression pattern of *nppa* shows a disturbed atrial morphology (Fig. 10).

Based on the reduction in the size and cell number of the ventricular cardiomyocytes, we also analyzed *ndrg4* expression in the *tbx2ab* morphants compared to wildtype embryos. Ndrg4 (N-myc downstream regulated gene 4) is a member of the NDRG family of proteins that regulate cellular differentiation. The *ndrg4* gene is expressed throughout the linear heart tube at low levels and by 48 hpf is mainly restricted to the ventricle. Loss of *ndrg4* leads to a loss of myocardial cell numbers due to proliferation defects (Qu et al., 2008). Analysis by *in situ* hybridization of *tbx2ab* morphants at 48 hpf suggests a clear decrease in the *ndrg4* transcript levels compared to wildtype embryos (Fig. 10). We carried out qPCR experiments to compare *nppa* and *ndrg4* transcript levels at 1, 2, and 3 dpf. This verified that by 3 dpf the expression levels of *nppa* RNA are increased nearly 4-fold in *tbx2ab* morphants, which is significantly higher than found for either single morphant at that stage (Fig. 11). However, the qPCR data shows a similar increase in *nppa* levels in the *tbx2a* single morphants at 24 hpf (consistent with the *in situ* hybridization data, Fig. S5). Furthermore, although not maintained, both single morphants have higher transcript levels compared to wildtype by 3dpf (albeit significantly lower levels than the double morphant). These observations indicate that both genes can affect *nppa* levels, but that they also at least partially compensate for each other. The qPCR data documents a 2-fold relative decrease in *ndrg4* transcript levels for the double morphant at 3 dpf compared to wildtype (Fig. 11). Again, depletion of either single gene product causes a similar change in *ndrg4* transcript levels at earlier stages (in this case, a decrease) but this change compared to wildtype is only maintained by 3 dpf in the double morphants, suggesting again that the genes eventually compensate for each other. In summary, two growth factor genes known to regulate chamber growth may be regulated by both *tbx2a* and *tbx2b*, but each gene can compensate for loss of its sister gene product, which could explain at least in part why chamber abnormalities are only revealed by examining the double morphant embryos.

DISCUSSION

Functions for Tbx2 during non-chamber myocardial development are well established. In mice, Tbx2 is normally repressed by Tbx20, thereby establishing the boundary between proliferating chamber myocardium and the AVC (Cai et al., 2005; Singh et al., 2005; Stennard et al., 2005). Mis-expression of Tbx2 in the heart causes a block to chamber development. Likewise, over-expression of human TBX2 in zebrafish by injection of mRNA causes lack of chamber growth and disrupted looping (Ribeiro et al., 2007). However, gain-of-function approaches can in principle mask additional developmental roles that are stage-specific. We note that our results are not contradictory to the published literature, which documents clearly that *tbx2* is eventually restricted to non-chamber myocardium and in this context it clearly can repress proliferation. However, the previous studies evaluated *tbx2* function at a different developmental stage than we report here. Our work demonstrates that the expression patterns for *tbx2* genes is dynamic in the zebrafish, since both genes are expressed at low but readily quantifiable levels in cardiomyocytes at 24 hpf. However, by 48 hpf, the gene expression patterns become restricted to the presumptive AVC and Tbx2 inhibits cell proliferation at this time and place. Our results suggest that for zebrafish, in addition to repressing myocardial development in the AVC, *tbx2* also regulates an earlier stage of chamber development by promoting cardiomyocyte proliferation and regulating chamber size. Our study benefits by the fact that zebrafish have two distinct *tbx2* genes due to a genome-wide duplication event. During the course of evolution, the function of *tbx2* was shared between these two genes. Both genes have a similar expression pattern in the embryonic heart. In addition to their previously established expression in the AVC, they are also expressed early throughout myocardium of the linear heart tube. Knockdown of both *tbx2* genes leads to cardiac chamber size defects.

Tbx2 appears to regulate atrial and ventricular chamber development in different ways. In the developing ventricle *tbx2* promotes cell proliferation, so that when both gene products are depleted below a threshold the ventricle is smaller due to fewer cardiomyocytes, which can be attributed to decreased proliferation. This is consistent with previous studies that associate Tbx2 with growth control. One mechanism by which *tbx2* could regulate ventricular development is by activating expression of *ndrg4*, a gene involved in cell proliferation and differentiation. The *ndrg4* promoter has putative T-box binding sites, and so *tbx2* might regulate *ndrg4* directly. Although *ndrg4* transcript levels are relatively reduced in the double morphants by 3 dpf, it is not clear if this is functionally relevant to the ventricular phenotype, since at earlier stages *ndrg4* transcript levels are also reduced in either single morphant. There may be a developmental window particularly sensitive to *ndrg4* expression levels, and the gene might also be regulated at the post-transcriptional level. However, forced expression of *nrdg4* by RNA injection was not sufficient to rescue the ventricular phenotype (data not shown) so there are likely to be other, perhaps more relevant, *tbx2ab* targets required for normal ventricular cell proliferation. In contrast, in the developing atrium, *tbx2* restricts atrial size. This could be achieved by regulating cardiomyocyte cell size, consistent with the fact that atria in the *tbx2ab* morphants are enlarged, yet the cell number is normal. However, an equally plausible explanation is that cell shape is altered, for example cells may be flattened due to physiological forces or from stretch placed upon the atrium. Alterations in hemodynamic forces, for example caused by weakened contractility or reduced blood flow from a shortened ventricle, could affect the chamber morphology. Our attempts at higher resolution morphometrics were not conclusive. However, the change is associated in the morphants with an expanded domain and increased levels of transcripts encoding *nppa*, as early as 24 hpf. Whether this reflects a direct or indirect mechanism is unclear, but Tbx2 can form a complex *in vitro* with Nkx2.5 and repress *nppa* promoter activity (Habets et al., 2002). In summary, our experiments targeting simultaneously the depletion of both zebrafish *tbx2* genes has shown that, in addition to a key role in AVC development, the two *tbx2* genes encode an earlier and functionally redundant activity for regulating myocardial chamber development by promoting ventricular cell proliferation and restricting atrial chamber size. The previously described role of *tbx2* in AVC development appears to be conserved with mammals. Although not described, an earlier function for TBX genes in heart chambers could be conserved in mammals, if, as in zebrafish, *Tbx2* functions redundantly with a closely related sister gene, for example *Tbx3*.

EXPERIMENTAL PROCEDURES

Fish strains and microinjection

Zebrafish embryos were maintained at 28°C and staged as described (Westerfield, 1995). Wildtype fish are hybrids derived from a cross between AB and TU strains. The *myl7:dsRed-nuc* strain was kindly provided by Nathalia Holtzman.

Morpholinos and micro-injections

Morpholinos were designed to block translation or splicing and were obtained from the manufacturer, GeneTools, Inc. The MO2b (Gross and Dowling, 2005) morpholino was previously validated in the published studies and was confirmed to be effective when injected at 6 ng per embryo. A morpholino to *tbx2a* was validated in published studies (Ribeiro et al., 2007) and this was phenocopied by MO2a (GATCCAGTTTTCACAGCGAACGCTA). The MO2a oligomer has significant mis-match with the *tbx2b* sequence (Fig. S2) and was used at 4 ng. The MO2ab (ATGCACCGATGAGAGATCCAGTTTT) is 100% matched to both *tbx2a* and *tbx2b* transcripts and gave reproducible and consistent results when injected at 2ng/embryo.

Generation of chimeric RNAs

The following oligomers were designed to span the MO2ab binding sequence present in both genes. In addition the *tbx2a* sequence also contains the binding site for the specific MO2a site.

*tbx2a*F: 5′-AATTCggatgcaccgatgagagatccagttttcacagcgaacgctatggcGGTAC

*tbx2a*R: 5′-CgccatagcgttcgctgtgaaaactggatctctcatcggtgcatccG

*tbx2b*F: 5′-AATTCgtttgttggatgcaccgatgagagatccagtttttacaggGGTAC

*tbx2b*R: 5′-CcctgtaaaaactggatctctcatcggtgcatccaacaaacG

After annealing, each pair was cloned into the pEGFP-1 expression vector that was digested with EcoRI and KpnI, placing GFP in frame with the translation initiation sites. Inserts were transferred using XhoI and (blunted) NotI into the pCS2 expression vector (XhoI and SnaBI digested). RNA was generated *in vitro* using the Ambion SP6 mMessage protocol.

in situ hybridization

Whole-mount *in situ* hybridization was performed essentially as described (Alexander et al., 1998). Briefly, embryos were treated with 0.003% phenylthiourea (PTU) to prevent pigmentation. After fixation, embryos older than 24 hours were treated with 10 μg/ml proteinase K. Hybridization was performed at 70C, in 57% formamide buffer with digoxigenin-labeled RNA anti-sense probes. The probes used for *in situ* hybridization were prepared using either Sp6 or T7 polymerase and linearized templates. Antisense probes have been described for *myl7*, *amhc*, and *vmhc* (Reiter et al., 1999). To generate a probe for *nppa*, the following primers were used to isolate a 420 bp fragment from embryonic cDNA: nppaF: 5′-AGAGATGGCCGGGGGACTAA and nppaR: 5′-CCGAGGGTGCTGGAAGAC. The product was sub-cloned into the TOPO vector and antisense probe generated using Sp6 polymerase following EcoRV digestion. A full-length cDNA clone for *ndrg4* was purchased from OpenBiosystems (clone ID 7049397, accession number BC116615). The pExpress-1 vector was linearized with EcoRI and used to generate antisense probe using T7 polymerase.

BrdU assay

20mM BrdU/15% DMSO in E3 buffer solution (2 nl) was injected into the pericardial cavity of tricaine anesthetized embryos. Embryos were placed into fish system water and incubated at 28.5C for 1.5 hours. Embryos were then de-yolked and fixed in 4% PFA for 2 hours, transferred to methanol and stored at -20C overnight. Embryos were rehydrated in methanol:PBST (3:1, 1:1, 1:3) and twice in PBST for 5 min each. Embryos were subsequently treated with 10μg/ml proteinase K for 10 min, washed twice in PBST and fixed in 4% PFA for 20 min at room temperature. Embryos were washed 3 times in H_20, twice with 2N HCl, and incubated for 1 hour in HCl at room temperature. They were rinsed 5-7 times with PBST and blocked for 30 min (0.2% Roche blocking reagent, 10% fetal bovine serum, and 1% DMSO in PBST) followed by incubation with 1:100 dilution of Anti-BrdU-Fluorescein monoclonal antibody (Roche) and 1:20 dilution of MF20 antibody (Iowa Hybridoma Bank) for 2 hour at room temperature in blocking solution. They were then washed 5 times with PBST for 10 min each and incubated with a 1:500 dilution of secondary anti-mouse IgG2b antibody (Alexa fluor 568) in PBST solution at 4C overnight. Finally, they were washed 5 times with PBST 10 min each and stored at 4C in the dark. The S46 antibody was also obtained from the Iowa Hybridoma Bank and used at 1:50 concentration. In this case the anti-BrdU IgG2a monoclonal antibody from TheromoScientific was used at a 1:100 dilution and secondary antibodies were AlexaFluor®

488 goat anti-mouse IgG2a and AlexaFluor® 568 goat anti-mouse IgG1 (Invitrogen), both used at 1:500 dilution. Embryos were positioned in methylcellulose for imaging.

Heart measurements

The *myl7:gfp* morphant and control embryos were anesthetized in tricaine until hearts stopped beating, positioned in methylcellulose and photographed under fluorescence. Because the embryos were tricaine-overdosed the hearts are considered to be in diastole. The area comprising cardiac chambers was outlined and measured using Zeiss AxioVision4.8 software. To count cardiomyocytes, *myl7:dsRed-nuc* control or morpholino-injected embryos were flat mounted on standard microscope slides. Z-stack sections of hearts were imaged in order to visualize and manually count all cardiomyocyte nuclei.

Quantitative RT/PCR

RNA was isolated from approximately 25 embryos using a Qiagen RNeasy mini kit and cDNA was synthesized using the Qiagen SuperscriptRT III kit. The cDNA was diluted 1:20 in qPCR reactions using the Roche SyberGreen kit. Samples that were analyzed on a Roche light cycler 480 instrument and test genes normalized to the *18s* ribosomal RNA gene transcripts. All samples were prepared in triplicate, and each experiment was repeated at least 3 times using independent batches of embryos. The PCR cycle conditions were 95C for 5 minutes, (94C for 10 seconds, 55C for 10 seconds, and 72C for 10 seconds) for 40 cycles. The Ct value data were analyzed using the $2^{-\Delta\Delta T}$ method (Livak and Schmittgen, 2001).

The following primers were used for qPCR:

*18s*F: TCGCTAGTTGGCATCGTTTATG

*18s*R: CGGAGGTTCGAAGACGATCA

*nppa*F: ACAGAGACCGAGAGGAAGCA

*nppa*R: CTTCGGGTCGACAATAGGAG

*ndrg4*F: TTGAGTGCAATTCCAAGCTG

*ndrg4*R: GTGTGATCTGAGGCATTCCA

Supplementary Material

Refer to Web version on PubMed Central for supplementary material.

Acknowledgments

The authors are grateful to Bernice Morrow and her laboratory for assistance in the design and testing of *tbx2* morpholinos. We also thank Nathalia Holtzman for providing the *myl7:dsRed-nuc* reporter strain. We thank Gabriel Rosenfeld for providing unpublished RNA-sequencing data from purified 24 hpf cardiomyocytes. Kellie McCartin provided outstanding fish husbandry. We also thank Bernice Morrow, Rick Kitsis, Nick Sibinga, Florence Marlow, and members of the Evans laboratory for helpful comments during the course of these studies.

Grant Sponsor: National Institutes of Health, HL064282

REFERENCES

Abrahams A, Parker MI, Prince S. The T-box transcription factor Tbx2: its role in development and possible implication in cancer. IUBMB Life. 2010; 62:92–102. [PubMed: 19960541]

Alexander J, Stainier DY, Yelon D. Screening mosaic F1 females for mutations affecting zebrafish heart induction and patterning. Dev Genet. 1998; 22:288–299. [PubMed: 9621435]

Auman HJ, Coleman H, Riley HE, Olale F, Tsai HJ, Yelon D. Functional modulation of cardiac form through regionally confined cell shape changes. PLoS Biol. 2007; 5:e53. [PubMed: 17311471]

Bakkers J, Verhoeven MC, Abdelilah-Seyfried S. Shaping the zebrafish heart: from left-right axis specification to epithelial tissue morphogenesis. Dev Biol. 2009; 330:213–220. [PubMed: 19371733]

Boogerd CJ, Moorman AF, Barnett P. Protein interactions at the heart of cardiac chamber formation. Ann Anat. 2009; 191:505–517. [PubMed: 19647421]

Bruneau BG, Nemer G, Schmitt JP, Charron F, Robitaille L, Caron S, Conner DA, Gessler M, Nemer M, Seidman CE, Seidman JG. A murine model of Holt-Oram syndrome defines roles of the T-box transcription factor Tbx5 in cardiogenesis and disease. Cell. 2001; 106:709–721. [PubMed: 11572777]

Cai CL, Zhou W, Yang L, Bu L, Qyang Y, Zhang X, Li X, Rosenfeld MG, Chen J, Evans S. T-box genes coordinate regional rates of proliferation and regional specification during cardiogenesis. Development. 2005; 132:2475–2487. [PubMed: 15843407]

Chapman DL, Garvey N, Hancock S, Alexiou M, Agulnik SI, Gibson-Brown JJ, Cebra-Thomas J, Bollag RJ, Silver LM, Papaioannou VE. Expression of the T-box family genes, Tbx1-Tbx5, during early mouse development. Dev Dyn. 1996; 206:379–390. [PubMed: 8853987]

Chi NC, Shaw RM, De Val S, Kang G, Jan LY, Black BL, Stainier DY. Foxn4 directly regulates tbx2b expression and atrioventricular canal formation. Genes Dev. 2008; 22:734–739. [PubMed: 18347092]

Christoffels VM, Hoogaars WM, Tessari A, Clout DE, Moorman AF, Campione M. T-box transcription factor Tbx2 represses differentiation and formation of the cardiac chambers. Dev Dyn. 2004; 229:763–770. [PubMed: 15042700]

Fong SH, Emelyanov A, Teh C, Korzh V. Wnt signalling mediated by Tbx2b regulates cell migration during formation of the neural plate. Development. 2005; 132:3587–3596. [PubMed: 16033799]

Gross JM, Dowling JE. Tbx2b is essential for neuronal differentiation along the dorsal/ventral axis of the zebrafish retina. Proc Natl Acad Sci U S A. 2005; 102:4371–4376. [PubMed: 15755805]

Habets PE, Moorman AF, Clout DE, van Roon MA, Lingbeek M, van Lohuizen M, Campione M, Christoffels VM. Cooperative action of Tbx2 and Nkx2.5 inhibits ANF expression in the atrioventricular canal: implications for cardiac chamber formation. Genes Dev. 2002; 16:1234–1246. [PubMed: 12023302]

Harrelson Z, Kelly RG, Goldin SN, Gibson-Brown JJ, Bollag RJ, Silver LM, Papaioannou VE. Tbx2 is essential for patterning the atrioventricular canal and for morphogenesis of the outflow tract during heart development. Development. 2004; 131:5041–5052. [PubMed: 15459098]

Hoogaars WM, Barnett P, Moorman AF, Christoffels VM. T-box factors determine cardiac design. Cell Mol Life Sci. 2007; 64:646–660. [PubMed: 17380306]

Joziasse IC, van de Smagt JJ, Smith K, Bakkers J, Sieswerda GJ, Mulder BJ, Doevendans PA. Genes in congenital heart disease: atrioventricular valve formation. Basic Res Cardiol. 2008; 103:216–227. [PubMed: 18392768]

Klopocki E, Neumann LM, Tonnies H, Ropers HH, Mundlos S, Ullmann R. Ulnar-mammary syndrome with dysmorphic facies and mental retardation caused by a novel 1.28 Mb deletion encompassing the TBX3 gene. Eur J Hum Genet. 2006; 14:1274–1279. [PubMed: 16896345]

Li QY, Newbury-Ecob RA, Terrett JA, Wilson DI, Curtis AR, Yi CH, Gebuhr T, Bullen PJ, Robson SC, Strachan T, Bonnet D, Lyonnet S, Young ID, Raeburn JA, Buckler AJ, Law DJ, Brook JD. Holt-Oram syndrome is caused by mutations in TBX5, a member of the Brachyury (T) gene family. Nat Genet. 1997; 15:21–29. [PubMed: 8988164]

Liu CX, Shen AD, Li XF, Jiao WW, Bai S, Yuan F, Guan XL, Zhang XG, Zhang GR, Li ZZ. Association of TBX5 gene polymorphism with ventricular septal defect in the Chinese Han population. Chin Med J (Engl). 2009; 122:30–34. [PubMed: 19187613]

Livak KJ, Schmittgen TD. Analysis of relative gene expression data using real-time quantitative PCR and the 2(-Delta Delta C(T)). Method. Methods. 2001; 25:402–408.

Mahlamaki EH, Barlund M, Tanner M, Gorunova L, Hoglund M, Karhu R, Kallioniemi A. Frequent amplification of 8q24, 11q, 17q, and 20q-specific genes in pancreatic cancer. Genes Chromosomes Cancer. 2002; 35:353–358. [PubMed: 12378529]

Merscher S, Funke B, Epstein JA, Heyer J, Puech A, Lu MM, Xavier RJ, Demay MB, Russell RG, Factor S, Tokooya K, Jore BS, Lopez M, Pandita RK, Lia M, Carrion D, Xu H, Schorle H, Kobler JB, Scambler P, Wynshaw-Boris A, Skoultchi AI, Morrow BE, Kucherlapati R. TBX1 is responsible for cardiovascular defects in velo-cardio-facial/DiGeorge syndrome. Cell. 2001; 104:619–629. [PubMed: 11239417]

Paxton C, Zhao H, Chin Y, Langner K, Reecy J. Murine Tbx2 contains domains that activate and repress gene transcription. Gene. 2002; 283:117–124. [PubMed: 11867218]

Qu X, Jia H, Garrity DM, Tompkins K, Batts L, Appel B, Zhong TP, Baldwin HS. Ndrg4 is required for normal myocyte proliferation during early cardiac development in zebrafish. Dev Biol. 2008; 317:486–496. [PubMed: 18407257]

Reiter JF, Alexander J, Rodaway A, Yelon D, Patient R, Holder N, Stainier DY. Gata5 is required for the development of the heart and endoderm in zebrafish. Genes and Dev. 1999; 13:2983–2995. [PubMed: 10580005]

Ribeiro I, Kawakami Y, Buscher D, Raya A, Rodriguez-Leon J, Morita M, Rodriguez Esteban C, Izpisua Belmonte JC. Tbx2 and Tbx3 regulate the dynamics of cell proliferation during heart remodeling. PLoS One. 2007; 2:e398. [PubMed: 17460765]

Schoenebeck JJ, Yelon D. Illuminating cardiac development: Advances in imaging add new dimensions to the utility of zebrafish genetics. Semin Cell Dev Biol. 2007; 18:27–35. [PubMed: 17241801]

Sinclair CS, Adem C, Naderi A, Soderberg CL, Johnson M, Wu K, Wadum L, Couch VL, Sellers TA, Schaid D, Slezak J, Fredericksen Z, Ingle JN, Hartmann L, Jenkins RB, Couch FJ. TBX2 is preferentially amplified in BRCA1- and BRCA2-related breast tumors. Cancer Res. 2002; 62:3587–3591. [PubMed: 12097257]

Singh MK, Christoffels VM, Dias JM, Trowe MO, Petry M, Schuster-Gossler K, Burger A, Ericson J, Kispert A. Tbx20 is essential for cardiac chamber differentiation and repression of Tbx2. Development. 2005; 132:2697–2707. [PubMed: 15901664]

Stennard FA, Costa MW, Lai D, Biben C, Furtado MB, Solloway MJ, McCulley DJ, Leimena C, Preis JI, Dunwoodie SL, Elliott DE, Prall OW, Black BL, Fatkin D, Harvey RP. Murine T-box transcription factor Tbx20 acts as a repressor during heart development, and is essential for adult heart integrity, function and adaptation. Development. 2005; 132:2451–2462. [PubMed: 15843414]

Vance KW, Carreira S, Brosch G, Goding CR. Tbx2 is overexpressed and plays an important role in maintaining proliferation and suppression of senescence in melanomas. Cancer Res. 2005; 65:2260–2268. [PubMed: 15781639]

Westerfield, M. The Zebrafish Book: A Guide for the Laboratory Use of Zebrafish (Danio rerio). University Of Oregon Press; Eugene, OR: 1995.

Yamagishi H, Maeda J, Hu T, McAnally J, Conway SJ, Kume T, Meyers EN, Yamagishi C, Srivastava D. Tbx1 is regulated by tissue-specific forkhead proteins through a common Sonic hedgehog-responsive enhancer. Genes Dev. 2003; 17:269–281. [PubMed: 12533514]

Yelon D. Cardiac patterning and morphogenesis in zebrafish. Dev Dyn. 2001; 222:552–563. [PubMed: 11748825]

Zaffran S, Frasch M. Early signals in cardiac development. Circ Res. 2002; 91:457–469. [PubMed: 12242263]

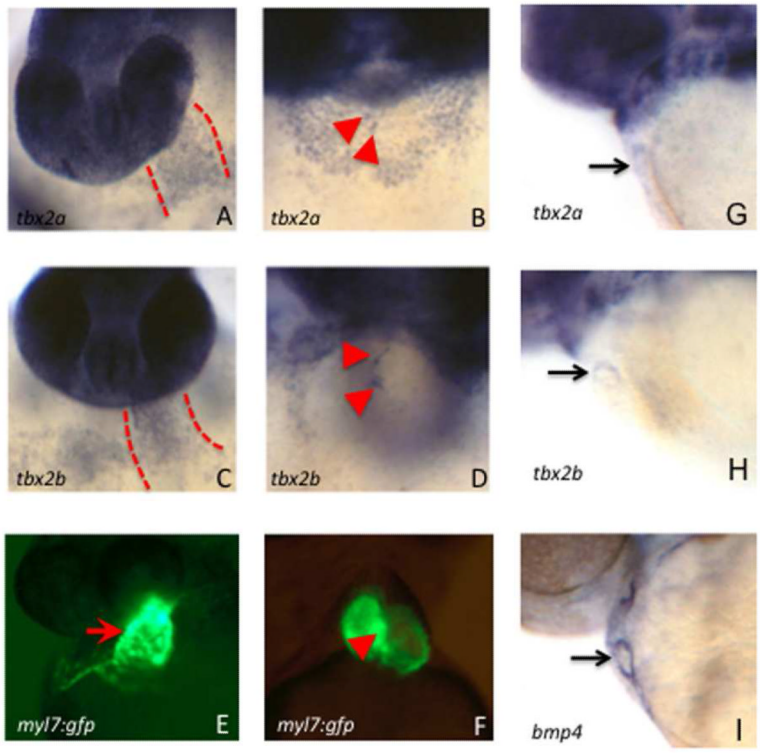

Fig. 1. Both *tbx2a* and *tbx2b* are expressed in the primitive heart tube and transcripts become restricted to the AVC by 2 dpf

Shown are representative embryos (n > 30 for each) analyzed by *in situ* hybridization to detect transcripts for *tbx2a* (A, B, G), *tbx2b* (C, D, H), or the AVC marker bmp4 (I). In addition to strong staining in the head, transcripts are readily detected in the primitive heart tube at 36 hpf (A, C, between the dashed lines) and subsequently in the AVC at 3 dpf (B, D, arrowheads marking the cushion tissue on either side of the AVC). Also shown for purpose of orientation are similarly staged *myl7:gfp* transgenic embryos that show the position of the heart tube at 36 hpf (E) and the AVC at 3 dpf (F). The restriction to the AVC can be seen starting already at 2 dpf, compared to bmp4 (G-I). Control sense strand probes failed to generate any detectable signal under the identical conditions (not shown).

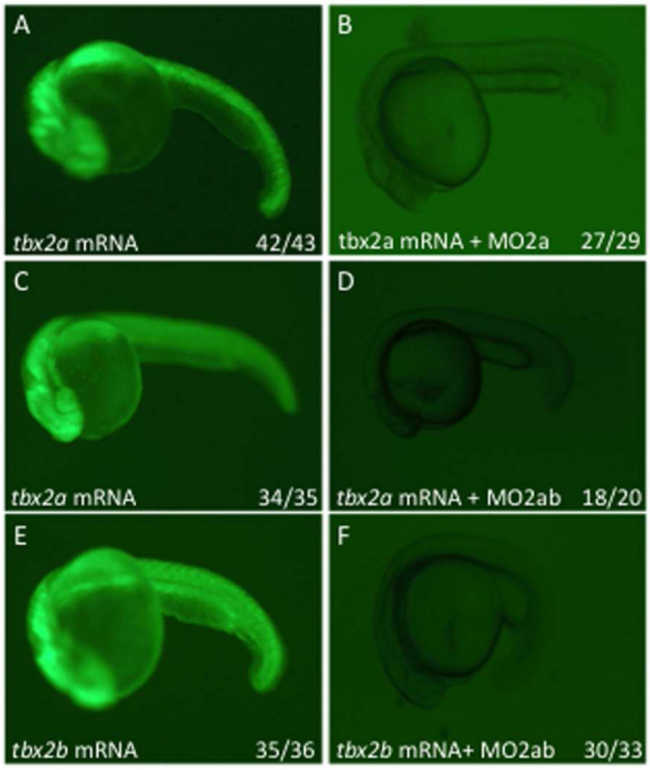

Fig. 2. A single morpholino targets a matched sequence in both *tbx2* genes

Embryos were injected at the one cell stage with 100 pg of *tbx2a-gfp* (A-D) or *tbx2b-gfp* (E-F) RNA which leads to strong fluorescence throughout the embryo at 24 hpf (A, C, E). This signal is completely blocked by co-injection of MO2a (B) or MO2ab (D, F). Note that the previously validated MO2b is not used in this assay, because it is a splice-blocker. However, MO2a does not block expression of the *tbx2b-gfp* transcript (not shown). For each sample n>25.

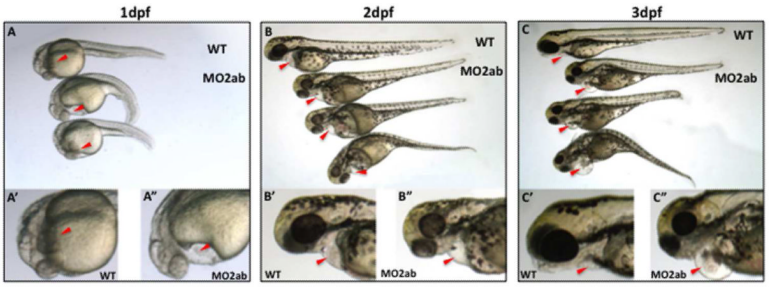

Fig. 3. The *tbx2ab* morphants display pericardial edema by 1 dpf and develop a severe cardiomyopathy

Shown are representative wildtype (top) and morphant embryos at 1 dpf (A), 2 dpf (B) and 3 dpf (C) showing increasingly dysmorphic hearts. Panels below are closer views of wildtype (‘) and morphant (‘’) embryos. Arrowheads mark the hearts. In each case n >100 embryos, and essentially 100% of the *tbx2ab* morphants show pericardial edema by 1 dpf, which is rarely seen in the single morphants.

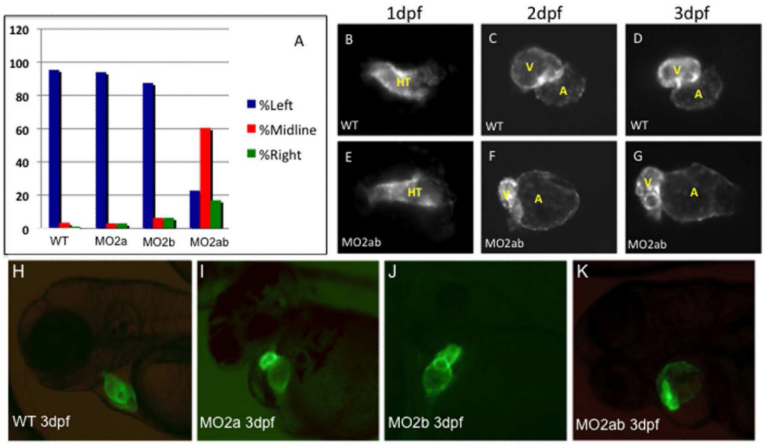

Fig. 4. Chamber morphogenesis is disrupted in the tbx2ab morphants

(A) Unlike single morphants, the *tbx2ab* double morphants show a heart tube jogging phenotype at 24 hpf. Wildtype and morphant embryos were evaluated at 24 hpf for the position of the primitive heart tube and scored as jogging left (normal, blue bars, right (green bars), or remaining midline (red bars). The Y axis indicates percentage of wildtype (WT), *tbx2a* morphant (MO2a), *tbx2b* morphant, or *tbx2ab* double morphant embryos. For each sample n = 50. (B-G) Cardiac morphogenesis is visualized by imaging expression of the *myl7:gfp* transgenic reporter gene in wildtype (WT, top panels) or *tbx2ab* morphants (MO2ab, lower panels), at 1 dpf (B, E), 2 dpf (C, F) or 3 dpf (D, G). HT indicates the heart tube, while V marks the ventricle and A marks the atrium. Note that the heart tube shape is relatively normal at 1 dpf but is markedly altered in chamber morphology by 2 or 3 dpf. Each panel shows the heart of a representative embryo. For each sample, n>100. The large atrium, small ventricle phenotype was scored in 110/172 *tbx2ab* morphants (64%). (H-K). The *tbx2ab* double morphants have distinct alterations in chamber morphology. Shown are representative wildtype (A), *tbx2a* morphant (B), *tbx2b* morphant (C), or *tbx2ab* double morphant (D) embryos at 3 dpf in the *myl7:gfp* background. While hearts of the single morphants do not loop properly, due to emerging defects in AVC development at this stage, the chamber sizes, although variation was noted, are similar to those of wildtype embryos. In contrast, chamber sizes in the double morphant are significantly disturbed. Over 100 embryos were analyzed for each, taken from multiple independent experiments.

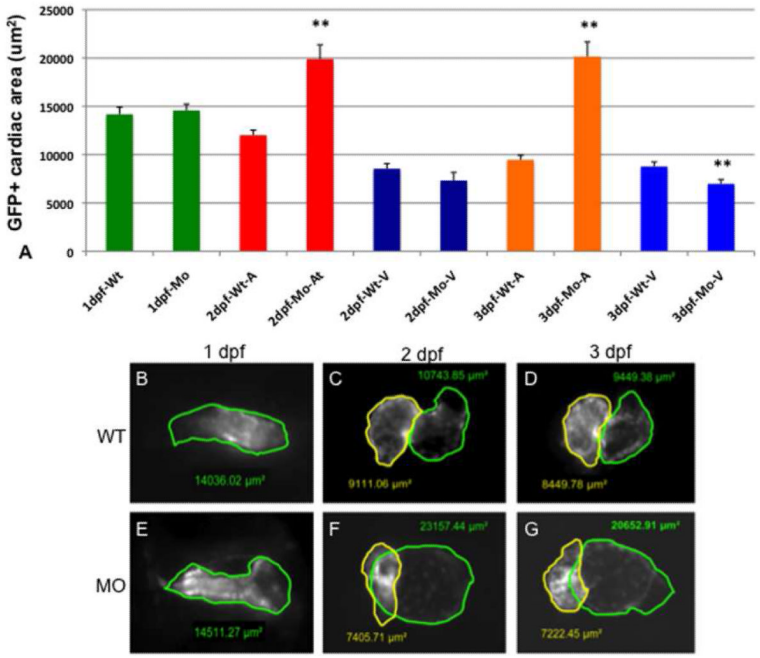

Fig. 5. Chamber sizes are altered in the *tbx2ab* morphants

Hearts were imaged in wildtype or *tbx2ab* double morphant embryos and the area of atrial and ventricular chambers was outlined and measured. The top panel (A) shows the quantification from representative embryos at 1 dpf, 2 dpf, or 3 dpf as indicated. Also as indicated, the measurement was in wildtype (WT) or morphant (MO), either in the heart tube (1 dpf, green), or for the atrium (A) or ventricle (V). In each case n is at least 10. Lower panels show representative images of wildtype and *tbx2ab* morphant hearts at 1 dpf (B, E), 2 dpf (C, F) and 3 dpf (D, G). In B and E the heart tube is outlined in green. In C, D, F, and G, yellow outlines the ventricle and green outlines the atrium. The ** indicates statistical significance compared to wildtype, according to Student's t-test, $p<0.01$.

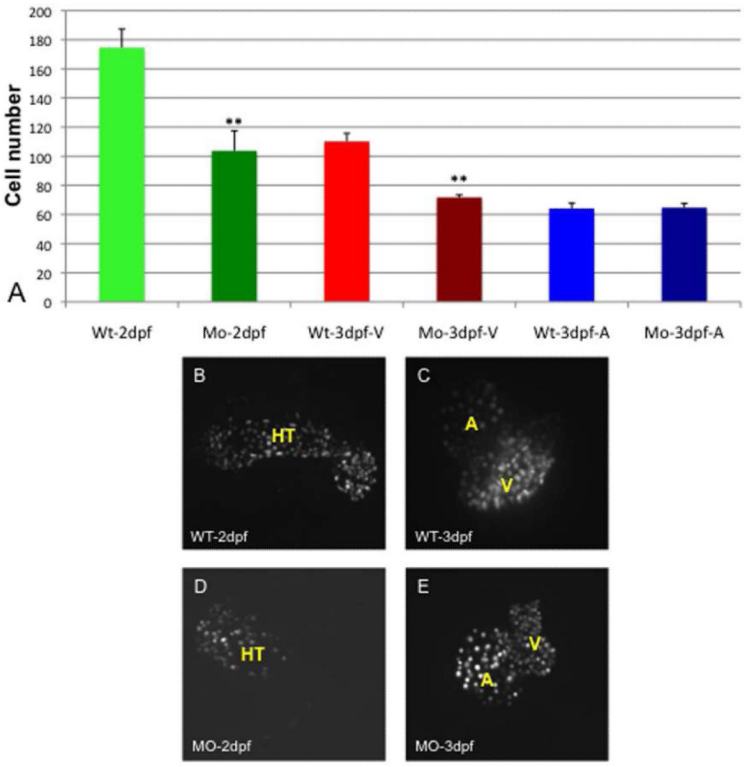

Fig. 6. The number of cardiomyocytes in *tbx2ab* morphants compared to wildtype is not different in the expanded atrium, but is relatively decreased in smaller ventricles

Hearts were imaged using embryos from the *myl7:dsRed-nuc* reporter line and numbers of cardiomyocytes counted manually in Z-stack sections. The top panel (A) shows the quantification of data for wildtype (WT) or double morphant embryos (Mo) at 2 dpf or 3 dpf as indicated. Also as indicated, the cells were counted in the heart tube (HT) at 2 dpf or specifically in the ventricle (V) or atrium (A) at 3 dpf. The ** indicates statistical significance compared to wildtype, according to Student's t-test, $p<0.01$. Lower panels show representative images of wildtype (WT) or *tbx2ab* morphants (MO) at 2 dpf (B, D) and 3 dpf (C, E). For each measurement n is at least 10.

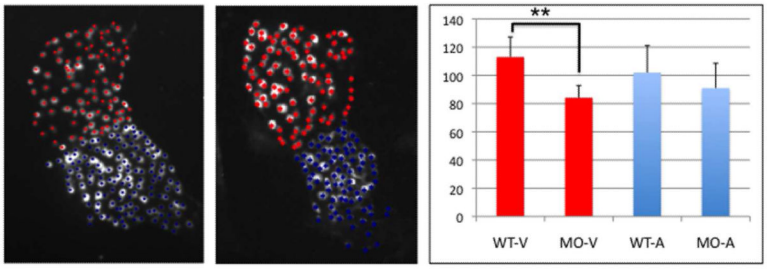

Fig. 7. The *tbx2ab* morphant has fewer ventricular cardiomyocytes by 2 dpf

Shown are representative hearts from wildtype (A) or *tbx2ab* morphant (B) embryos derived from the *myl7:dsRed-nuc* reporter line. Flat-mounted embryos were chosen that displayed a clear constriction at the position of the presumptive AVC and were imaged by confocal microscopy. Based on this morphological distinction, individual cells were marked as ventricular (red) or atrial (blue) and quantified as shown in the chart (C). For each sample n = 4, and this was reproducible evaluating independent batches of embryos. The morphant ventricle (but not the atrium) has significantly fewer cardiomyocytes (indicated on the Y-axis) compared to wildtype ($p<0.01$, according to Students t-test).

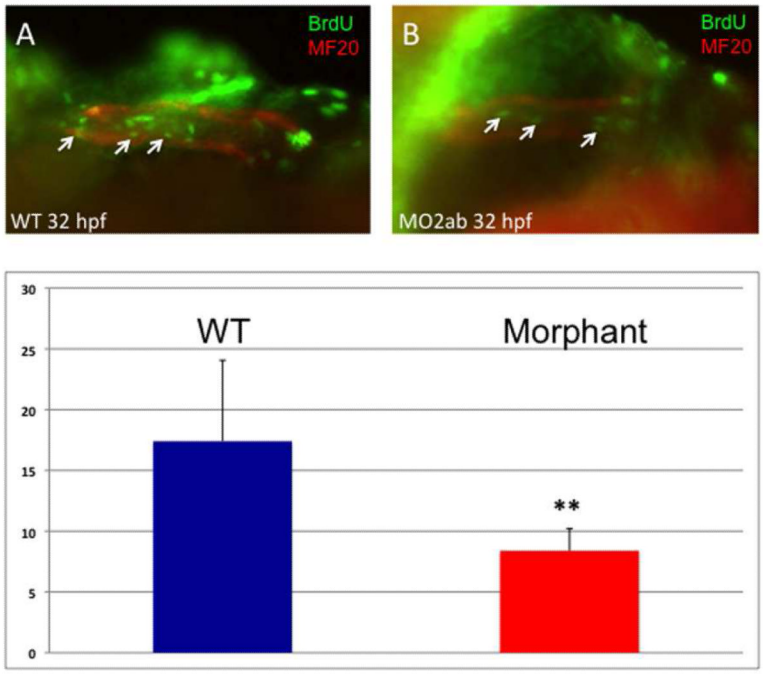

Fig. 8. Cardiomyocyte proliferation is decreased in the *tbx2ab* morphants

Embryos were pulse-labeled with BrdU, and after being fixed, were co-stained to detect BrdU+ cells (green) and MF20+ cardiomyocytes (red). Hearts were imaged and the yellow (double positive) cells counted (examples indicated by the small arrows). The top panels show representative wildtype (A) and morphant (B) embryos at ~32 hpf. The lower panel (C) shows quantification of the average BrdU+ cardiomyocytes, in each case from several randomly chosen embryos, n = 5. The ** indicates statistical significance compared to wildtype, according to Student's t-test, $p<0.02$. This experiment was repeated several times and reproducibly showed significantly decreased relative levels of BrdU+ cardiomyocytes in morphants, although the actual number of double-labeled cells varies depending on the efficiency of BrdU labeling.

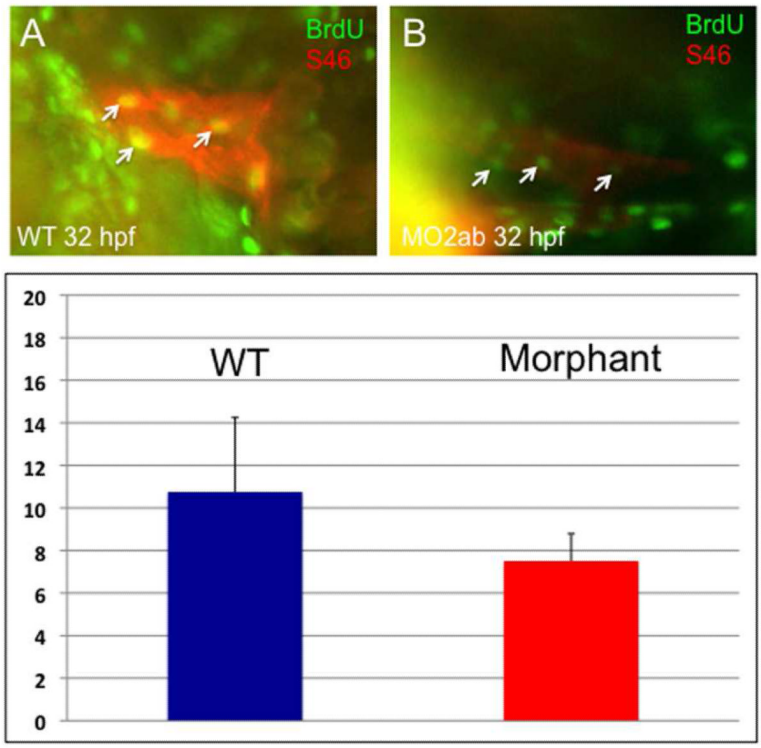

Fig. 9. Cardiomyocyte proliferation is not decreased in the atrium of *tbx2ab* morphants

Embryos were pulse-labeled with BrdU, and after being fixed, were co-stained to detect BrdU+ cells (green) and S46+ atrial cardiomyocytes (red). Hearts were imaged and the yellow (double positive) cells counted (examples indicated by the small arrows). The top panels show representative wildtype (A) and morphant (B) embryos at ~32 hpf. The lower panel (C) shows quantification of the average BrdU+ cardiomyocytes, in each case from several randomly chosen embryos, n = 4. According to Student's t-test, p=0.13. The result is consistent with the fact that the atrium is not altered in cell numbers.

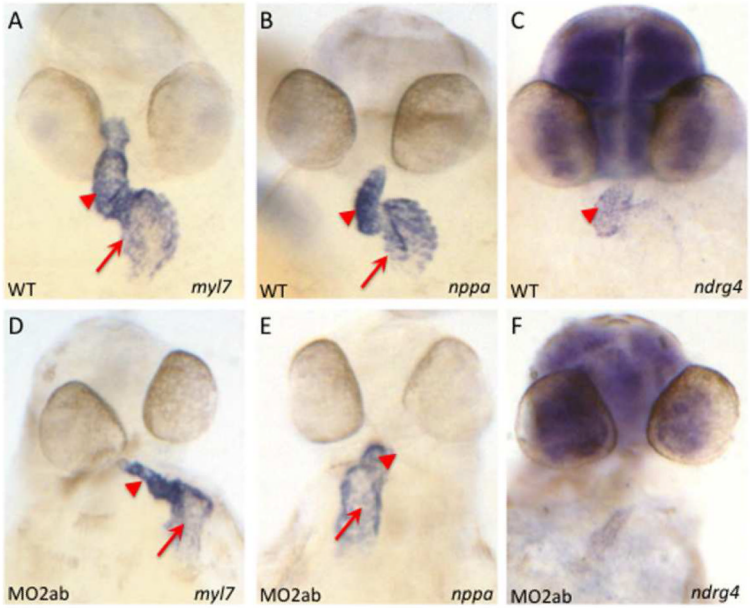

Fig. 10. Expression patterns for known chamber growth regulators are altered in the *tbx2ab* double morphant

Shown are representative embryos examined by *in situ* hybridization for expression of transcripts for *myl7* to indicate cardiomyocytes, and for the growth factors *nppa*, or *ndrg4* as indicated, in wildtype (A-C) and *tbx2ab* morphant (D-F) embryos at 2 dpf. Arrows indicate the atrial expression domain and arrowheads mark ventricular expression domain. Note that transcript levels for *ndrg4* are reduced in the presumptive ventricle. For each panel n is at least 20.

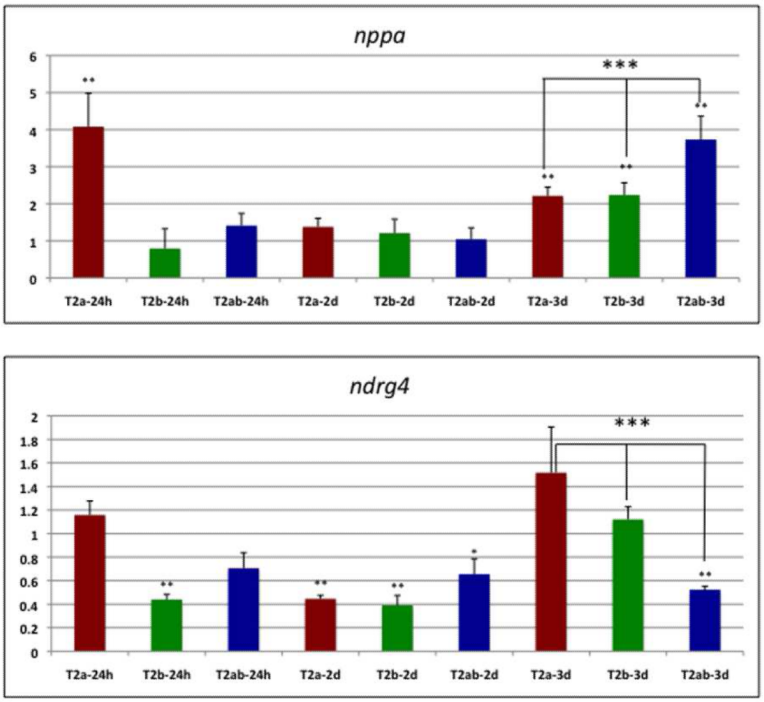

Fig. 11. Expression levels for *nppa* and *ndrg4* are significantly altered at 3 dpf in double *tbx2ab* morphants compared to single morphants

Shown are results from qPCR assays (n is at least 4 for each sample) for single *tbx2a* (T2a), *tbx2b* (T2b) or double *tbx2ab* (T2ab) morphants at 24 hpf (24h), 2 dpf (2d), or 3 dpf (3d), as indicated. Each sample was normalized to levels of transcripts derived from the *18s* rRNA gene, and the average plotted relative to values obtained in control wildtype embryos (set at 1). The top panel shows quantification of *nppa* transcript levels, and the bottom panel shows measurements for *ndrg4* transcripts. ** indicates that the *nppa* transcript values were significantly increased compared to wildtype for the *tbx2a* morphant at 24 hpf and for either single morphant and the double morphant at 3 dpf ($p<0.01$), and that *ndrg4* transcript levels are significantly decreased compared to wildtype for the *tbx2b* morphant at 24 hpf, both single and double morphants at 2 dpf (* indicates $p<0.05$ for the double morphant), and only the double morphant at 3 dpf ($p<0.01$). Importantly, *** above the brackets indicates that at 3 dpf, the double morphant is significantly increased for *nppa* transcript levels compared to either single morphant, and significantly decreased for *ndrg4* compared to the *tbx2b* morphant ($p<0.05$). Note that for the *tbx2a* single morphant there was more variation in *ndrg4* transcript levels, but if anything they were higher, and are therefore clearly trending to the same conclusion (in this case $p<0.08$). Statistical significance was determined according to Student's t-test.